DOI: 10.1002/cmdc.201300531

Effects of the Tumor-Vasculature-Disrupting Agent Verubulin and Two Heteroaryl Analogues on Cancer Cells, Endothelial Cells, and Blood Vessels

Katharina Mahal,[a] Marcus Resch,[b] Ralf Ficner,[b] Rainer Schobert,[a] Bernhard Biersack,*[a] and Thomas Mueller*[c]

Two analogues of the discontinued tumor vascular-disrupting agent verubulin (Azixa®, MPC-6827, **1**) featuring benzo-1,4-dioxan-6-yl (compound **5a**) and *N*-methylindol-5-yl (compound **10**) residues instead of the *para*-anisyl group on the 4-(methylamino)-2-methylquinazoline pharmacophore, were prepared and found to exceed the antitumor efficacy of the lead compound. They were antiproliferative with single-digit nanomolar IC_{50} values against a panel of nine tumor cell lines, while not affecting nonmalignant fibroblasts. Indole **10** surpassed verubulin in seven tumor cell lines including colon, breast, ovarian, and germ cell cancer cell lines. In line with docking studies indicating that compound **10** may bind the colchicine binding site of tubulin more tightly ($E_{bind} = -9.8$ kcal mol^{-1}) than verubulin ($E_{bind} = -8.3$ kcal mol^{-1}), **10** suppressed the formation of vessel-like tubes in endothelial cells and destroyed the blood vessels in the chorioallantoic membrane of fertilized chicken eggs at nanomolar concentrations. When applied to nude mice bearing a highly vascularized 1411HP germ cell xenograft tumor, compound **10** displayed pronounced vascular-disrupting effects that led to hemorrhages and extensive central necrosis in the tumor.

Introduction

Tumor blood vessels are a therapeutic target as they are fundamentally different from normal vasculature.[1,2] Vascular-targeting agents may belong to either of two groups: antiangiogenic compounds[3,4] which address factors that regulate the neo-formation of blood vessels or vascular-disrupting agents (VDA)[5,6] that destroy irregular tumor blood vessels. VDA are particularly interesting, as they often exhibit an immediate impact on the vasculature of tumors provoking their collapse after only a few applications. Most VDA are small molecules derived from natural lead compounds such as the combretastatins A,[7] plantal stilbene metabolites that bind to the colchicine binding site of tubulin and cause extensive cytoskeletal rearrangements of the microtubule and the actin backbones of endothelial cells.[8] Examples of this type are fosbretabulin[9,10] and AVE8062,[11,12] a phosphate and a serinyl prodrug of combretastatin A-4, respectively, and the combretastatin A-1 derivative OXi4503.[13] More recently, combretastatin A derivatives with imidazole, oxazole, or related heterocycles were developed that retain the vascular-disrupting effect of the lead compound while showing an enhanced cytotoxicity.[14–17] Other heterocyclic VDA, structurally remote from the archetypal natural VDA blueprints, were also identified. Verubulin (Azixa®, MPC-6827, **1**), a *para*-anisidyl-substituted quinazoline, exhibits vascular-disrupting effects coupled with strong apoptosis induction in tumor cells, including multidrug resistant cells. It is also capable of penetrating the blood brain barrier. Although it had successfully passed a phase IIb clinical trial for glioblastoma multiforme[18–20] the proprietor, Myrexis Inc., decided in 2011 to suspend any further development of **1** for economic reasons, only. As earlier competition assays with **1** and proven tubulin binders had suggested that it might bind to the colchicine or a nearby binding site, we now prepared and studied a series of analogues of **1** that bore benzoxacycles and indoles, heterocycles that figure prominently in other synthetic antimitotic agents.[21–23] Herein we report on the effects of **1** and of two derivatives with superior efficacy against tumor cells on the propensity of endothelial cells to form blood vessel-like tubular structures and on real blood vessels in hen egg models and xenograft tumors. The affinity of these three compounds to tubulin and the cytoskeleton of nonmalignant and cancer cells was ascertained by docking studies, in vitro binding assays, and immunofluorescent cell staining.

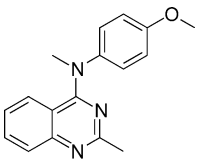
Azixa

[a] K. Mahal, Prof. Dr. R. Schobert, Dr. B. Biersack
Organic Chemistry Laboratory, University of Bayreuth
Universitätsstraße 30, 95440 Bayreuth (Germany)
E-mail: bernhard.biersack@uni-bayreuth.de

[b] Dr. M. Resch, Prof. Dr. R. Ficner
Department of Molecular Structural Biology
Georg August University Göttingen
Justus-von-Liebig-Weg 11, 37077 Göttingen (Germany)

[c] Dr. T. Mueller
Department of Internal Medicine IV, Oncology/Hematology
Martin Luther University, Halle-Wittenberg, 06120 Halle (Germany)
E-mail: thomas.mueller@medizin.uni-halle.de

Supporting information for this article is available on the WWW under http://dx.doi.org/10.1002/cmdc.201300531.

Results and Discussion

Chemistry

A series of 4-aminoquinazolines with benzo-1,4-dioxan-6-yl (**5a**), benzo-1,3-dioxolan-5-yl (**5b**), and benzofuran-5-yl (**5c**) residues were prepared by alkylation of the respective methyl aryl amines **4a**–**c** with 4-hydroxy-2-methylquinazoline in the presence of BOP[24] and DBU (Scheme 1). The amines **4**[25–27]

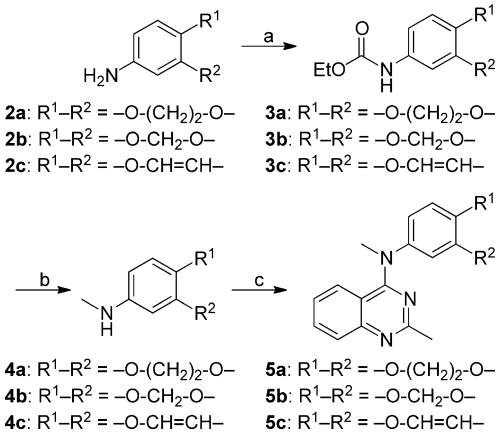

Scheme 1. Synthesis of quinazoline derivatives **5**. *Reagents and conditions*: a) EtOCOCl, Et_3N, THF, RT, 4 h, 78–95%; b) $LiAlH_4$, THF, reflux, 1 h, 79–94%; c) 2-methyl-4-hydroxyquinazoline, BOP, PhOPh, DBU, MeCN, RT, 16 h, 21–31%.

were obtained by conversion of the primary amines **2** to the carbamates **3** with ethyl chloroformate and reduction of **3** with $LiAlH_4$.

Scheme 2 depicts the synthesis of 2-methyl-4-[*N*-methyl-*N*-(1-methylindol-5-yl)]aminoquinazoline **10**. *N*-Methyl-5-nitroindole **6** was protected at C3 by chlorination with NCS to give compound **7**. Reduction of the nitro group with Zn/HCl and acylation of the resulting amine with ethyl chloroformate afforded carbamate **8**. This was reduced to methyl amine **9** by $LiAlH_4$. Analogous to compounds **4**, the amine **9** was coupled with 4-hydroxy-2-methylquinazoline in the presence of BOP and then dechlorinated via Pd-catalyzed hydrogenation to yield compound **10**.

Biological evaluation

The antiproliferative activities of compounds **5a**–**c** and **10** were evaluated first by MTT assays[28] with cells of highly proliferative 518A2 melanoma, chemosensitive HCT-116 colon, and multidrug resistant MCF-7/Topo breast carcinomas, as well as with hybrid Ea.hy926 endothelial cells and nonmalignant human foreskin fibroblasts (HF). The benzo-1,4-dioxane **5a** and the *N*-methylindole **10** were highly efficacious against all cancer cell lines with IC_{50} (72 h) values ranging from 0.4 to 1.0 nM, values not significantly

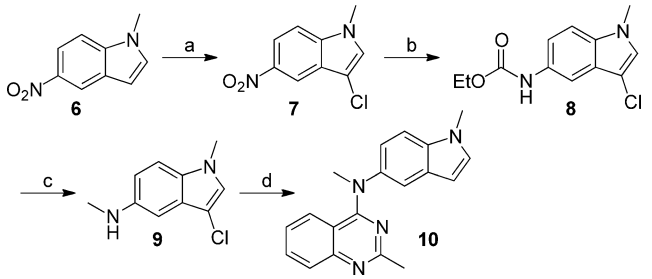

Scheme 2. Synthesis of *N*-(methylindolyl)aminoquinazoline **10**. *Reagents and conditions*: a) NCS, MeCN, RT, 4 h, 60%; b) Zn/HCl, THF, RT, 10 min, then EtOCOCl, Et_3N, THF, RT, 4 h, 61%; c) $LiAlH_4$, THF, reflux, 1 h, 87%; d) 2-methyl-4-hydroxyquinazoline, BOP, PhOPh, DBU, MeCN, RT, 16 h, then H_2, 10% Pd/C, MeOH, RT, 2 h, 32%.

different from **1**. Endothelial Ea.hy926 cells were also affected at nanomolar concentrations (72 h) whereas normal fibroblasts were not affected by compounds **5a** and **10** at concentrations of up to 10 μM. The derivatives **5b** and **5c** were less antiproliferative by one order of magnitude in all cells tested (Table 1). Next, the most active compounds **1**, **5a**, and **10** were tested against a second panel comprising two related testicular germ cell tumor cell lines,[29] the chemosensitive H12.1 and the drug-resistant 1411HP, as well as the colon cancer cell lines HT-29, DLD-1, and HCT-8, and the ovarian cancer cell line A2780.[30] Generally, indole **10** was marginally more antiproliferative against all six cancer cell lines than **1**. For the sensitive A2780 ovarian cancer cell line it even reached a sub-nanomolar IC_{50} (96 h) value. Compound **5a** exhibited a lower, though still impressive, activity with IC_{50} (96 h) values <6 nM for all cancer cell lines tested.

For an assessment of the effects of the new verubulin analogues on endothelial cells we used the hybrid endothelial cell

Table 1. Inhibitory concentrations of compounds **1**, **5a**–**c**, and **10** when applied to human foreskin fibroblasts (HF), Ea.hy926 hybrid endothelial cells, and various cancer cells.

Cell Line	IC_{50} [nM][a]				
	1	**10**	**5a**	**5b**	**5c**
HF[b]	>10000	>10000	>10000	–	–
Ea.hy926[c]	>1000	>1000	>1000	–	–
Ea.hy926[b]	30±10	27±5	43±8	–	–
518A2[b]	0.3±0.1	0.4±0.1	0.9±0.1	7.6±3.7	30±9
HCT-116[b]	0.2±0.0	1.0±0.0	0.8±0.1	9.0±0.6	11±1
MCF-7/Topo[b]	1.3±0.6	1.0±0.0	1.0±0.0	51±17	29±2
H12.1[d]	1.8±0.1	1.7±0.1	4.3±0.6	–	–
1411HP[d]	2.6±0.5	2.0±0.2	5.8±0.2	–	–
HT-29[d]	1.7±0.1	1.4±0.1	3.4±1.1	–	–
HCT-8[d]	1.8±0.1	1.6±0.1	4.2±1.1	–	–
DLD-1[d]	1.8±0.1	1.7±0.1	4.7±0.6	–	–
A2780[d]	1.4±0.1	0.9±0.2	1.8±0.1	–	–

[a] Values are derived from dose–response curves obtained by measuring the percentage of viable cells relative to untreated controls after exposure to test compounds using: [b] MTT (72 h exposure), [c] MTT (24 h exposure), or [d] SRB (96 h exposure) assays. Values represent the mean±SD of four independent experiments (–: not measured). Human cancer cell lines: 518A2 melanoma, HCT-116 colon, HT-29 colon, HCT-8 colon, DLD-1 colon, MCF-7/Topo breast, A2780 ovarian carcinoma, H12.1, and 1411HP germ cell tumors.

line Ea.hy926, which is easier to passage and cultivate than primary endothelial cells such as human umbilical vein endothelial cells (HUVEC). The flow cytometric analysis revealed a two- to threefold increase of cells in the G2/M phase following incubation for 24 h with 10 nM of **1**, **5a**, or **10** (Figure 1, Table 2). Compared with **1** and **5a** the onset of this effect was somewhat retarded in the case of **10**. The fact that only 10% of the cells were apoptotic after 24 h, as assessed from the sub-G1 events, suggests that the pronounced growth inhibition observed in the MTT and SRB assays after 96 h is owed not to a direct induction of apoptosis but to this G2/M cell-cycle arrest. Other tubulin-targeting agents such as taxol, vinblastine, and combretastatin A-4 are known to cause such a mitotic arrest in primary cells as a result of an aberrant or impaired development of functional spindle microtubules and the disruption of the normal chromosome attachment to the mitotic spindle apparatus.[31] A prolonged mitotic arrest can eventually lead to the induction of apoptosis, or alternatively, cells may also exit from mitosis by dividing into daughter cells with polyploid or other abnormal genome content.[31]

To determine how the microtubule dynamics of Ea.hy926 endothelial cells respond to treatment with compounds **1**, **5a**, or **10**, their microtubule cytoskeleton was visualized by immunofluorescent staining (Figure 2). Exposure for 24 h to 10 nM of the compounds caused a complete disruption of the highly organized tubulin filaments and a diffuse distribution of the stained microtubule subunits throughout the whole of the cytosol. The cells also showed an aberrant cell morphology and a distinct membrane blebbing. In principal, this blebbing could be the result of an actin-mediated cellular stress response as in the case of endothelial cells treated with combretastatin A-4.[32] Alternatively, it could be "apoptotic blebbing", as a consequence of apoptosis induction. Here, in the case of Ea.hy926 cells treated with **1**, **5a**, or **10** the morphological changes are indicative of alterations in the actin cytoskeleton. As a proof we stained their actin filaments with a fluorescent phalloidin conjugate and analyzed the subcellular distribution of filamentous actin (F-actin, Figure 2). Although most actin filaments in untreated control cells were of the cortical type, concentrated near the plasma membrane fringe, the F-actin in cells exposed to 10 nM of **1**, **5a**, or **10** was organized in trusses of stress fibers, scattered all over the cell body. The majority of treated cells also featured a markedly increased cytosolic volume and two contiguous or separated nuclei. We therefore assume that the mechanism by which verubulin (**1**) and its analogues **5a** and **10** induce growth inhibition is at least partially mediated by inhibiting cell division due to the loss of a func-

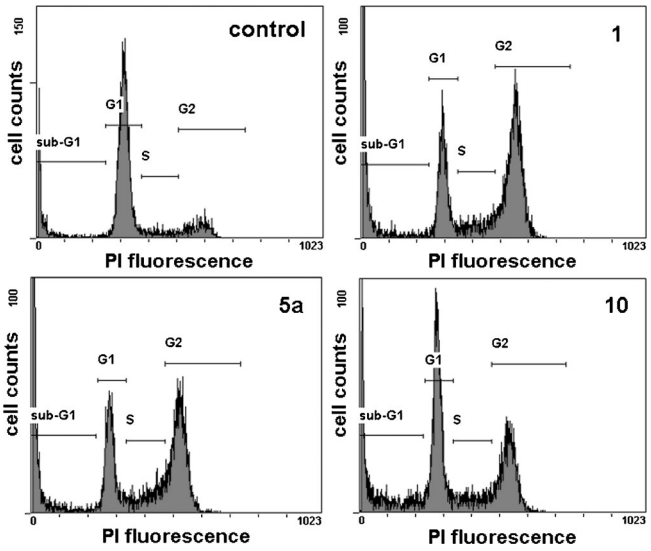

Figure 1. Effect of **1**, **5a**, and **10** (10 nM, 24 h) on the cell cycle of Ea.hy926 cells. Typical cell-cycle profiles and percentage of treated cells in G1, S, and G2 phases as well as sub-G1 events (apoptotic cells) as obtained by flow cytometry after DNA staining with propidium iodide; control: DMSO.

Table 2. Percentage of Ea.hy926 endothelial cells in G1, S, and G2/M cell-cycle phases and the proportion of apoptotic cells (sub-G1) after treatment with compounds **1**, **5a**, or **10**.

Phase	Cell Count [%][a]			
	Control	**1**	**5a**	**10**
sub-G1	14.5 ± 0.1	24.1 ± 2.4	24.9 ± 0.7	21.1 ± 3.4
G1	66.2 ± 0.8	22.4 ± 0.7	22.3 ± 1.7	41.3 ± 3.0
S	6.8 ± 0.3	9.5 ± 1.0	10.6 ± 2.3	10.7 ± 0.5
G2/M	12.6 ± 0.3	44.0 ± 1.6	42.2 ± 4.6	26.9 ± 1.0

[a] Determined by flow cytometry. Cells were treated with the test compound at 10 nM for 24 h; control cells were treated with DMSO only. Values represent the mean ± SD of $n = 3$ independent experiments.

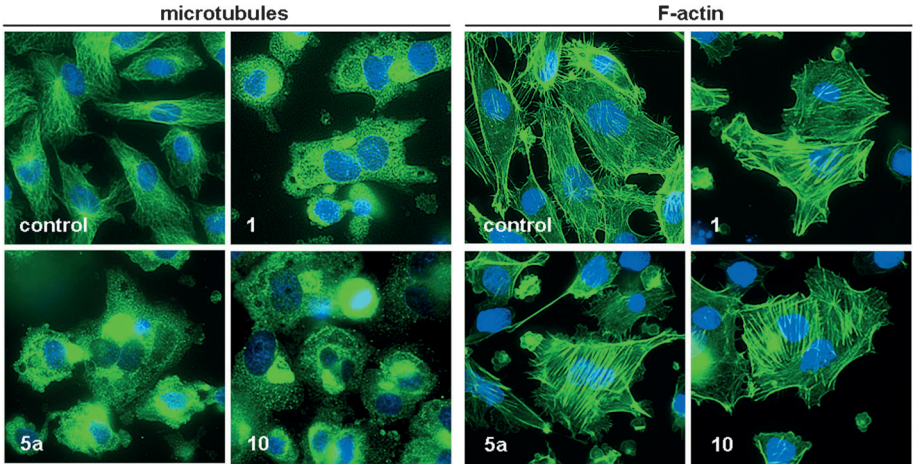

Figure 2. Effect of **1**, **5a**, and **10** (10 nM, 24 h) on the cytoskeletal organization of microtubules (left panels) and F-actin (right panels) in Ea.hy926 endothelial cells. Nuclei (blue) were counterstained with DAPI (400× magnification).

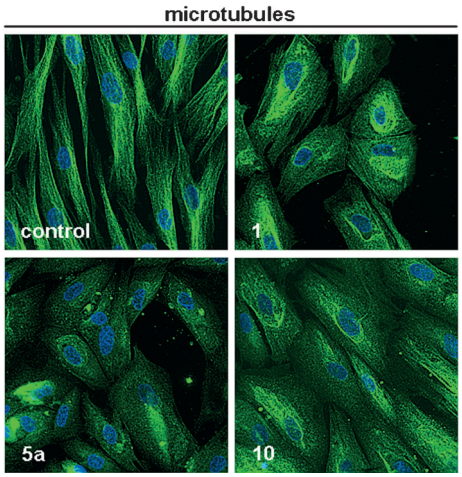

Figure 3. Effect of **1**, **5a**, and **10** (100 nM, 24 h) on the microtubule cytoskeleton of human fibroblasts (HF). Nuclei (blue) were stained with DAPI (400× magnification).

tional cytoskeletal organization.[31] Immunofluorescent staining of microtubules in nonmalignant fibroblasts (HF cells) treated with 100 nM of **1**, **5a**, or **10** revealed a pronounced disruption of the microtubule cytoskeleton, yet no dinucleated cells (Figure 3). Thus, the test compounds predominantly affect rapidly proliferating cells.

As mentioned in the introductory section, the molecular mechanism of action of verubulin **1** is still largely unknown. This includes the precise mode of its interaction with tubulin which is believed to take place near the colchicine binding site at the α-/β-tubulin heterodimeric interface.[20] We now studied the molecular interaction of compounds **1**, **5a**, and **10** with tubulin in two different ways: first, kinetically, with purified tubulin and the tubulin polymerization assay kit by Cytoskeleton, and then by in silico prediction, via molecular docking. Figure 4 shows the time dependency of tubulin polymerization in samples containing 3 μM of the test compounds. Interestingly, indole **10** was a less effective polymerization inhibitor than **1** and **5a**, despite its stronger growth inhibitory effect in most of the tested cancer cell lines and its pronounced effect

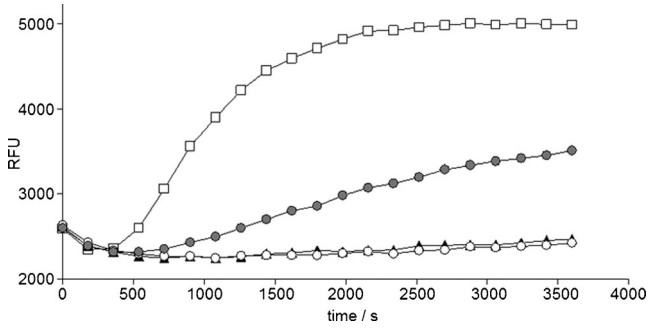

Figure 4. Effects of **1** (▲), **5a** (○), or **10** (●), each at 3 μM, on the polymerization of tubulin as ascertained with a fluorescence-based assay kit from Cytoskeleton (control, □). Data are representative of four independent experiments; RFU: relative fluorescence units as a measure of the degree of polymerization.

on the cytoskeleton. Tubulin interaction seems to be just one of many factors that contribute to the overall impact on the cell and it is probably not decisive for the viability of cells that can exit mitotic arrest without immediate death.

Next, molecular docking studies were conducted to gain insight into the possible tubulin binding mode and to gauge the binding energy of the quinazolines **1**, **5a**, and **10**. The crystal structure of bovine dimeric tubulin (PDB ID: 1SA0, 100% sequence identity to human tubulin) complexed with colchicine and Mg^{2+}-coordinated GDP and GTP was used to dock the quinazolines in the colchicine binding site.[33] Docking studies with the suite AutoDock Vina[34] predicted them to bind in an orientation analogous to colchicine with the aryl ring, that is, anisyl (**1**), benzo-1,4-dioxanyl (**5a**), or *N*-methylindolyl ring (**10**), proximal to Cys-β241 (Figure 5) and its respective heteroatom,

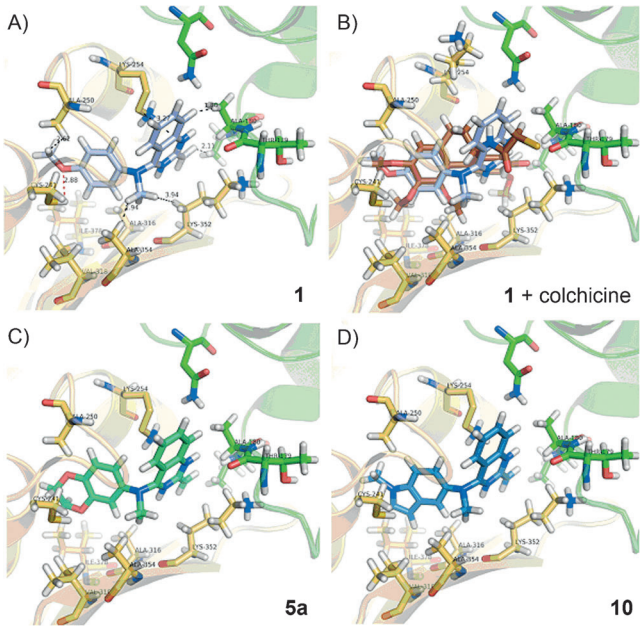

Figure 5. Docking of verubulin (**1**) (A, B), **5a** (C), and **10** (D) into the crystal structure of bovine tubulin (PDB ID: 1SA0) with α-tubulin shown in green and β-tubulin in ochre. Important amino acid residues are depicted as sticks and labeled accordingly. Secondary structure elements are semitransparent. A) Putative hydrogen bonding (red dashed lines) and van der Waals interactions (black dashed lines) of **1** to bovine tubulin. B) Overlay of the docking positions of **1** (calculated) and of colchicine (from X-ray crystal structure; brown). C) Optimized docking position of **5a**. D) Optimized docking position of **10**.

O or N, within typical hydrogen bond distance from the SH-group of Cys-β241 (Figure 5A,C). A similar binding situation was previously found for combretastatin A-4 analogues.[35,36] In addition, the A ring including the *para*-methoxy group of **1**, the dioxane and phenyl rings of **5a**, and the *N*-methylindole moiety of **10** are stabilized by van der Waals interactions within the hydrophobic pocket made up by the side chains of Leu-β248, Ala-β250, Ala-β316, Val-β318, Ala-β354, and Ile-β378 (Figure 5A,C,D). This hydrophobic network mimics that of colchicine's trimethoxyphenyl ring (Figure 5B).[33] Furthermore, the methyl group at the bridging exocyclic amino nitrogen

Table 3. Calculated binding energies of colchicine and quinazolines **1**, **5a**, and **10** to the colchicine binding site of tubulin.

Ligand	E_{bind} [kcal mol^{-1}][a]
colchicine	−9.0
1	−8.3
5a	−9.0
10	−9.8

[a] Values calculated by AutoDock Vina.[31]

atom favorably interacts with the Lys-β352 β-methylene and the side chains of Ala-β316 and Ala-β354. Remarkably, the ammonium residue of Lys-β254 can enter into a cation–π interaction with the quinazoline rings of **1**, **5a**, and **10**.[37,38] Table 3 summarizes the calculated binding energies. Compounds **5a** and **10** are predicted to bind more strongly to tubulin than **1**, and indole **10** even more strongly than the lead compound colchicine. However, given a standard error of 2.8 kcal mol^{-1} for AutoDock Vina calculations,[31] these binding enthalpies should not be over interpreted. A permissible conclusion from these studies is that the new compounds are able to bind in a similar orientation and at least as strongly to tubulin as the known verubulin (**1**).

We further assessed the antivascular properties in vitro using tube formation assays[39,40] which are based on the propensity of endothelial cells to form complex cord- or tube-like networks when grown on a basement membrane matrix (matrigel). Relative to untreated control cells which undergo a continuous migration and differentiation into highly ordered structures, cultures of hybrid endothelial Ea.hy926 cells exposed to 25 nM of **1**, **5a**, or **10** showed a retraction of the stretched intercellular connections after only 6 h (Figure 6). After 24 h there were clusters of vital cells without tubular outgrowth indicating that the essential morphological alterations, migrations, and differentiation processes were severely hindered because of cytoskeletal damage and reorganization induced by **1**, **5a**, or, most distinctly, by **10**.

These effects were reproducible in vivo when **1**, **5a**, or **10** were applied topically to the vascularized chorioallantoic membrane (CAM) of fertilized chicken eggs.[41] Disruption of small blood vessels as well as hemorrhages as a result of leaking or broken vessels were observed within the first 6 h (Figure 7). Even after 24 h hours there was no sign of regeneration or neo-formation of blood vessels within the silicon ring that confined the area of application.

Finally, we investigated the vascular-disrupting effect of compound **10** on established tumor vessels in vivo using our model of the highly vascularized 1411HP nude mouse xeno-

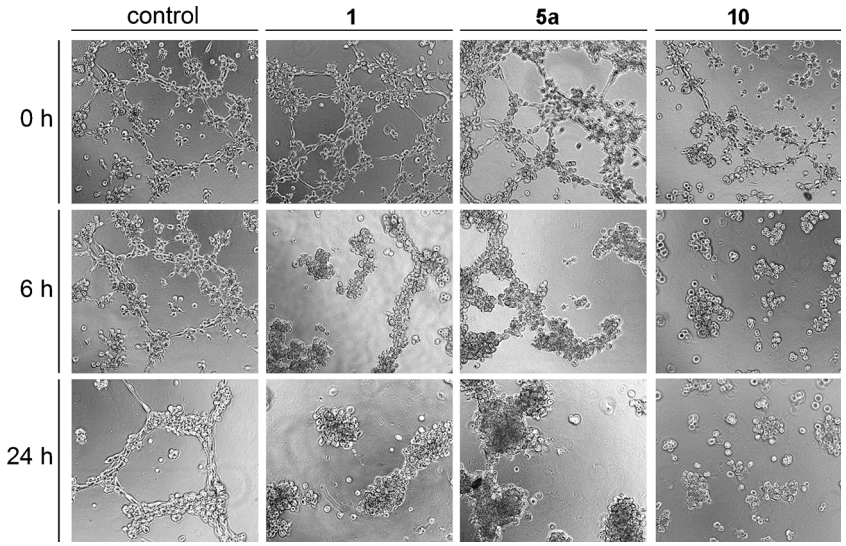

Figure 6. Formation or destruction of tubular networks in Ea.hy926 endothelial cells grown on thin matrigel layers when treated with compound **1**, **5a**, **10** (each at 25 nM), or with DMSO (control) for the indicated incubation times. Images were taken with a light microscope (100× magnification).

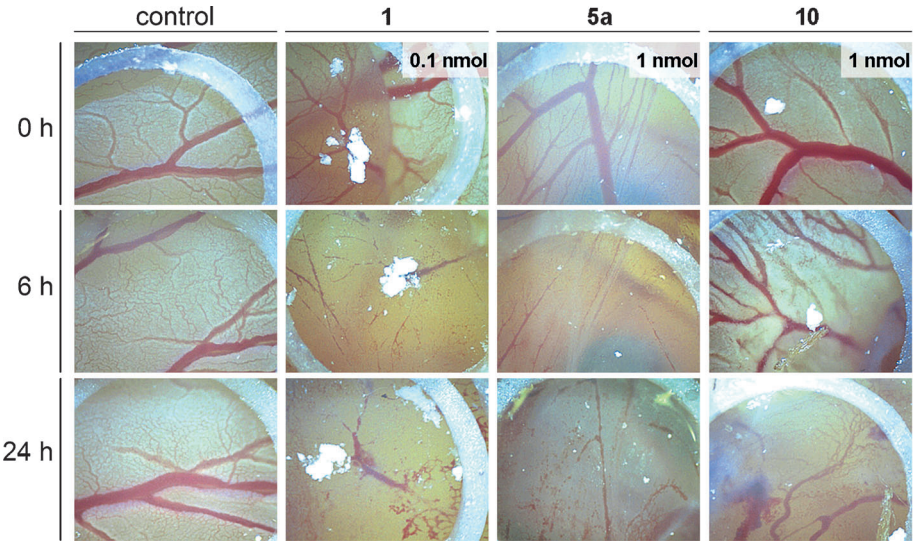

Figure 7. Effects of compounds **1** (0.1 nmol), **5a** (1.0 nmol), and **10** (1.0 nmol) on the blood vessels of the CAM of fertilized chicken eggs inside a ring of silicon foil (5 mm diameter) after 0, 6, and 24 h; control: DMSO. Images are representative of three independent assays (60× magnification).

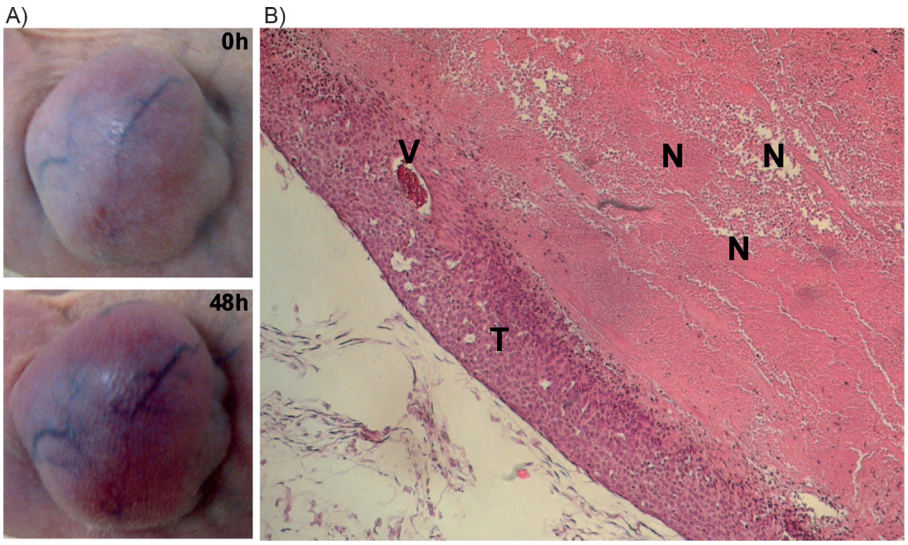

Figure 8. Vascular disrupting effect of **10** in a 1411HP xenograft tumor. A) Discoloration of the tumor due to intratumoral hemorrhage. B) Lateral section of the tumor shown in A (bottom) after HE staining featuring a large necrotic core area (**N**) surrounded by a cortical layer of vital tumor cells (**T**) which encompasses intact blood vessels (**V**).

graft tumor.[17] As shown in Figure 8A, a single intraperitoneal dose of 5 mg kg^{-1} of **10** induced a strong discoloration of the entire tumor because of substantial intratumoral hemorrhage. A histological examination of the treated tumor revealed an extensive central necrosis and a persistent rim of surviving tumor cells, features that are usually observed upon treatment with VDA. No internal bleeding could be detected in the sacrificed mice.

Conclusions

We identified the microtubule and actin cytoskeletons as the main cellular targets of the discontinued antitumor drug candidate verubulin (**1**). The rapid and pronounced depolymerization of the microtubules of cancer cells by **1** and the formation of actin stress fiber networks in these led to a G2/M cell-cycle arrest and eventual cell death. These effects are similar to those described for other vascular-disrupting agents such as CA-4.[8,32,42] On a molecular level the strong affinity of **1** for tubulin could be demonstrated by in vitro polymerization assays with purified tubulin and by in silico docking experiments. The propensity of endothelial cells to form vasculature-like tubular networks was markedly attenuated by **1** and existing blood vessels in the chorioallantoic membrane (CAM) of fertilized hen eggs were destroyed by it.

Out of a series of new derivatives of **1** with heterocyclic appendages other than *para*-anisyl, two compounds **5a** and **10** stuck out. While addressing the same molecular targets, the cytotoxic effect of **10** in malignant cells was greater than that of **1**. More importantly, its vascular-disrupting effect in the tube formation assay was more distinct as was its tolerance by chicken embryos in the CAM assay. Application of doses higher than 0.5 nmol was lethal after 6 h only in the case of **1**. Treatment with the same amount of **5a** or **10** was far better tolerated by the chicken embryo and did not prevent it from growing and developing normally (Supporting Information, Table S1). In in vivo studies with mice bearing strongly vascularized 1411HP germ cell tumor xenografts, indole **10** caused extensive intratumoral hemorrhages and eventually necrosis due to long-lasting vascular occlusion (ischemia). The resulting necrotic core of the tumor was surrounded by a rim of persistent viable tumor cells as is typical of VDA in general.[42] Internal bleeding in the mice was not detected.

Experimental Section

Chemistry

2-Methyl-4-(*N*-benzodioxan-3-yl-*N*-methylamino)quinazoline (5a): 2-Methyl-4-hydroxyquinazoline (100 mg, 0.62 mmol) and BOP (393 mg, 0.89 mmol) were dissolved in acetonitrile (5 mL) and treated with diphenyl ether (108 μL, 0.68 mmol) and DBU (205 μL, 1.37 mmol). The solution was stirred at RT for 5 min before compound **4a** (370 mg, 2.24 mmol) was added. The reaction mixture was stirred at RT for 16 h. The solvent was evaporated and purification by column chromatography (silica gel 60; EtOAc/*n*-hexane, 1:1) gave **5a** as a colorless solid (40 mg, 21%): mp: 200 °C; R_f = 0.15 (EtOAc/*n*-hexane, 1:1); ^{1}H NMR (300 MHz, $CDCl_3$): δ = 2.69 (s, 3H), 3.54 (s, 3H), 4.2–4.3 (m, 4H), 6.60 (dd, ^3J = 8.6 Hz, ^4J = 2.6 Hz, 1H), 6.70 (d, ^4J = 2.6 Hz, 1H), 6.81 (d, ^3J 8.6 Hz, 1H), 6.9–7.0 (m, 1H), 7.10 (dd, ^3J = 7.7 Hz, ^4J = 2.0 Hz, 1H), 7.5–7.6 (m, 1H), 7.72 (dd, ^3J = 7.7 Hz, ^4J = 1.8 Hz, 1H); ^{13}C NMR (75.5 MHz, $CDCl_3$): δ = 26.4, 42.5, 64.3, 114.8, 115.0, 118.2, 119.2, 124.0, 126.2, 127.6, 131.7, 142.1, 144.3, 152.0, 161.6, 163.3 ppm; ATR-IR (neat): $\tilde{\nu}_{max}$ = 2968, 2928, 2875, 1614, 1587, 1564, 1547, 1492, 1464, 1448, 1434, 1381, 1352, 1308, 1278, 1245, 1229, 1180, 1155, 1125, 1099, 1063, 1049, 1035, 1007, 989, 937, 911, 885, 862, 827, 766, 748, 726, 687 cm^{-1}; MS (EI, 70 eV): *m/z* (%): 307 (100) $[M]^+$, 306 (73), 250 (14), 222 (28), 164 (44), 143 (42), 102 (43).

2-Methyl-4-(*N*-methyl-*N*-1-methylindol-5-ylamino)quinazoline (10): A solution of 2-methyl-4-hydroxyquinazoline (100 mg, 0.62 mmol) and BOP (393 mg, 0.89 mmol) in acetonitrile (5 mL) was treated with diphenyl ether (108 μL, 0.68 mmol) and DBU (205 μL, 1.37 mmol), stirred at RT for 5 min, and then treated with **9** (130 mg, 0.67 mmol). The reaction mixture was stirred at RT for 16 h. The solvent was evaporated and the residue was purified by column chromatography (silica gel 60; EtOAc/MeOH, 95:5). The obtained 3-chloroindol-5-ylaminoquinazoline (R_f 0.29, EtOAc) was separated from adhering benzotriazole impurities by extraction of the solid mixture with minute amounts of ethyl acetate. The yellow ethyl acetate phase was separated from the less soluble benzotriazole and concentrated in vacuo to leave the 3-chloroindol-5-ylaminoquinazoline. This was dissolved in methanol (10 mL), treated with 10% Pd/C (70 mg), and stirred at RT under hydrogen gas (1 atm) for 2 h. The resulting black suspension was filtered over Celite and the filtrate was concentrated in vacuo to afford the title com-

pound **10** as a yellow solid (60 mg, 32%): mp: 248 °C; ^{1}H NMR (300 MHz, MeOD): $\delta = 2.71$ (s, 3H), 3.79 (s, 3H), 3.86 (s, 3H), 6.48 (d, $^3J = 3.1$ Hz, 1H), 6.74 (d, $^3J = 8.6$ Hz, 1H), 6.9–7.0 (m, 1H), 7.14 (dd, $^3J = 8.6$ Hz, $^4J = 2.2$ Hz, 1H), 7.30 (d, $^3J = 3.1$ Hz, 1H), 7.5–7.6 ppm (m, 4H); ^{13}C NMR (75.5 MHz, MeOD): $\delta = 23.8$, 33.3, 45.0, 102.7, 112.6, 119.3, 120.4, 122.5, 126.7, 128.7, 131.0, 132.7, 135.1, 137.5, 139.3, 158.2, 162.7 ppm; ATR-IR (neat): $\tilde{\nu}_{max} = 3639$, 3343, 2948, 1623, 1608, 1588, 1569, 1528, 1488, 1424, 1389, 1366, 1338, 1271, 1242, 1196, 1162, 1108, 1084, 996, 829, 761, 737, 686 cm^{-1}; MS (EI, 70 eV): *m/z* (%): 302 (100) $[M]^+$, 301 (89), 286 (10), 159 (37), 144 (45), 130 (22), 102 (38), 77 (14).

Molecular docking studies

Coordinate files of the ligand structures were generated by the GlycoBioChem PRODRG2 Server (http://davapc1.bioch.dundee.ac.uk/prodrg/submit.html).[43] Molecular docking calculations were carried out with the AutoDock Vina software.[34] and Gasteiger partial charges[44] were calculated on ligand atoms using AutoDock Tools. The X-ray structure of the crystallized tubulin–colchicine complex (PDB ID: 1SA0) was downloaded from the Protein Data Bank (http://www.rcsb.org). Polar hydrogen atoms were added to the protein and Gasteiger partial charges were calculated. Water molecules, heteroatoms, and ligands were removed from the structure prior to docking calculations. Residues Lys-β254, Lys-β352, Asn-α101, Val-β318, and Ile-β378 were treated as flexible residues. Simulation boxes were centered on the originally crystallized ligand colchicine. A 17×23×19 Å simulation box and an exhaustiveness option of 1,000 were used in the docking calculations. Figures were prepared with the program PyMOL.[45]

Biological studies

Cell-cycle analyses: Ea.hy926 cells (1×10^5 mL) grown on six-well plates were treated with DMSO (control), **1**, **5a**, or **10** (10 nM, 24 h), fixed (70% EtOH, 1 h, 4 °C) and incubated with propidium iodide (PI; Carl Roth) staining solution (50 μg mL^{-1} PI, 0.1% sodium citrate, 50 μg mL^{-1} RNase A in PBS) for 30 min at 37 °C. The fluorescence intensity of 10,000 single cells at $\lambda_{em} = 620$ nm ($\lambda_{ex} = 488$ nm laser source) was recorded with a Beckman Coulter Cytomics FC 500 flow cytometer and analyzed for the distribution of single cells (%) to G1, S, or G2/M phases as well as for the content of sub-G1 (apoptotic) events (CXP software, Beckman Coulter).

Fluorescence labeling of microtubules and actin filaments: Ea.hy926 cells (1×10^5 mL) were grown on glass coverslips in 24-well plates, treated with DMSO (control), **1**, **5a**, or **10** (10 nM) for 24 h, fixed with 4% formaldehyde in PBS for 20 min at RT, and permeabilized with 1% BSA, 0.1% Triton X-100 (in PBS) for 30 min. Nonmalignant HF were treated with 100 nM of **1**, **5a**, or **10**. To visualize F-actin, coverslips were incubated with 1 U AlexaFluor®-488-conjugated phalloidin (Invitrogen) for 1 h at 37 °C. For microtubule staining, fixed and permeabilized cells were treated with a primary antibody against α-tubulin (anti-α-tubulin, mouse mAb, Invitrogen; 5 μg mL^{-1}) for 1 h (37 °C, 5% CO_2, 95% humidity) followed by incubation with the secondary antibody conjugated to the fluorescent AlexaFluor®-488 dye (goat anti-mouse IgG-AlexaFluor-488 conjugate, Invitrogen; 4 μg mL^{-1}) for 1 h at RT in the dark. The coverslips were then mounted in Mowiol 4-88-based mounting medium containing 2.5% (*w/v*) DABCO and 1 μg mL^{-1} DAPI (4′,6-diamidino-2-phenylindole) for counterstaining the nuclei. Fluorescence microscopic analysis of the effects on both cytoskeletal components was performed using the ZEISS Axio Imager.A1 microscope.

Tube formation assays:[39,40] The effect of **1**, **5a**, and **10** on the propensity of stimulated Ea.hy926 cells to form vascular-like tubular networks in vitro was assessed by growing the cells (0.5×10^6 mL) on thin matrigel (BD Biosciences) layers for 12 h and then treating them with DMSO (control) or 25 nM of the test compounds. Documentation by light microscopy after 6 h and 24 h (10× magnification, Axiovert 135, AxioCam MRc 5, ZEISS). MTT was additionally added to each well after 24 h to ensure that more than 80% of the remaining cells are vital.

Chorioallantoic membrane (CAM) assays:[41] Fertilized white leg horn chicken eggs (SPF eggs, VALO Biomedia) were incubated (37 °C, 50–60% humidity) and opened on day six by cutting a window of 2–3 cm diameter into the eggshell at the more rounded pole. Rings of silicon foil (Ø 5 mm) were placed on the developing CAM vessels, the windows were sealed with tape and the eggs were incubated for a further 12–18 h. 1 nmol or 0.1 nmol (10 μL of a 100 μM or 10 μM solution in ddH_2O) of **1**, **5a**, **10**, or vehicle (DMSO) were pipetted inside the silicon ring. The effects were documented after 0 h, 6 h, and 24 h post application with a microscope (60× magnification, Traveller).

Animal studies: The vascular-disrupting activity of **10** was studied on the established model of highly vascularized 1411HP xenograft tumors previously described.[17] This study was approved by the Laboratory Animal Care Committee of Sachsen-Anhalt, Germany. Nude mice (Harlan and Winkelmann, Borchen, Germany) received 5 mg kg^{-1} body weight of compound **10** by intraperitoneal injection and tumor discoloration was documented immediately and after 48 h with a Canon IXUS 50. For histological examination the tumors were explanted, fixed in 4% formalin, and embedded in paraffin. Hematoxylin/eosin staining of the tissue slices was performed according to standard protocols.

Supporting Information

Instruments used; syntheses, microanalytical and spectroscopic data of all new compounds; MTT and SRB assays; tubulin polymerization assays.

Abbreviations

BOP, benzotriazol-1-yloxy-tris(dimethylamino)phosphonium hexafluorophosphate; CA-4, combretastatin A-4; CAM, chorioallantoic membrane; DAPI, 4′,6-diamidino-2-phenylindole; DBU, 1,8-diazabicyclo[5.4.0]undec-7-ene; HE, hematoxylin-eosin; MTT, 3-(4,5-dimethylthiazol-2-yl)-2,5-diphenyltetrazolium bromide; PI, propidium iodide; SRB, sulforhodamine-B; VDA, vascular-disrupting agent.

Keywords: angiogenesis · antitumor agents · quinazolines · vascular-disrupting agents · verubulin

[1] D. McDonald, P. Choyke, *Nat. Med.* **2003**, *9*, 713–725.
[2] D. J. Chaplin, G. J. Dougherty, *Br. J. Cancer* **1999**, *80 (Suppl. 1)*, 57–64.
[3] N. Ferrara, R. S. Kerbel, *Nature* **2005**, *438*, 967–974.
[4] P. Carmeliet, R. K. Jain, *Nature* **2000**, *407*, 249–257.
[5] D. W. Siemann, *Cancer Treat. Rev.* **2011**, *37*, 63–74.
[6] J. W. Lippert III, *Bioorg. Med. Chem.* **2007**, *15*, 605–615.
[7] G. R. Pettit, S. B. Singh, E. Hamel, C. M. Lin, D. S. Alberts, D. Garcia-Kendall, *Experientia* **1989**, *45*, 209–211.
[8] C. Kanthou, G. M. Tozer, *Expert Opin. Ther. Targets* **2007**, *11*, 1443–1457.
[9] D. J. Chaplin, S. Hill, *Int. J. Radiat. Oncol. Biol. Phys.* **2002**, *54*, 1491–1496.

[10] C. J. Mooney, G. Nagaiah, P. Fu, J. K. Wasman, M. M. Cooney, P. S. Savvides, J. A. Bokar, A. Dowlati, D. Wang, S. S. Agarwala, S. M. Flick, P. H. Hartman, J. D. Ortiz, P. N. Lavertu, S. C. Remick, *Thyroid* **2009**, *19*, 233 – 240.
[11] A. Delmonte, C. Sessa, *Expert Opin. Invest. Drugs* **2009**, *18*, 1541 – 1548.
[12] G. Del Conte, R. Bahleda, V. Moreno, S. Damian, A. Perotti, N. Lassau, F. Farace, M. Ong, S. J. Stimpson, N. Tunariu, S. Micallef, B. Demers, C. Oprea, G. Capri, J.-C. Soria, C. Sessa, L. R. Molife, *J. Clin. Oncol.* **2012**, *30 (Suppl. Abstr.)*, 3080.
[13] H. W. Salmon, D. W. Siemann, *Clin. Cancer Res.* **2006**, *12*, 4090 – 4094.
[14] G. C. Tron, T. Pirali, G. Sorba, F. Pagliai, S. Busacca, A. A. Genazzani, *J. Med. Chem.* **2006**, *49*, 3033 – 3044.
[15] L. Wang, K. W. Woods, Q. Li, K. J. Barr, R. W. McCroskey, S. M. Hannick, L. Gherke, R. B. Credo, Y.-H. Hui, K. Marsh, R. Warner, J. Y. Lee, N. Zielinski-Mozng, D. Frost, S. H. Rosenberg, H. L. Sham, *J. Med. Chem.* **2002**, *45*, 1697 – 1711.
[16] K. Bonezzi, G. Taraboletti, P. Borsotti, F. Bellina, R. Rossi, R. Giavazzi, *J. Med. Chem.* **2009**, *52*, 7906 – 7910.
[17] R. Schobert, B. Biersack, A. Dietrich, K. Effenberger-Neidnicht, S. Knauer, T. Mueller, *J. Med. Chem.* **2010**, *53*, 6595 – 6602.
[18] N. Sirisoma, A. Pervin, H. Zhang, S. Jiang, J. A. Willardsen, M. B. Anderson, G. Mather, C. M. Pleiman, S. Kasibhatla, B. Tseng, J. Drewe, S. X. Cai, *J. Med. Chem.* **2009**, *52*, 2341 – 2351.
[19] N. Sirisoma, A. Pervin, H. Zhang, S. Jiang, J. A. Willardsen, M. B. Anderson, G. Mather, C. M. Pleiman, S. Kasibhatla, B. Tseng, J. Drewe, S. X. Cai, *Bioorg. Med. Chem. Lett.* **2010**, *20*, 2330 – 2334.
[20] S. Kasibhatla, V. Baichwal, S. X. Cai, B. Roth, I. Skvortsova, S. Skvortsov, P. Lukas, N. M. English, N. Sirisoma, J. Drewe, A. Pervin, B. Tseng, R. O. Carlson, C. M. Pleiman, *Cancer Res.* **2007**, *67*, 5865 – 5871.
[21] S. Arora, X. I. Wang, S. M. Keenan, C. Andaya, Q. Zhang, Y. Peng, W. J. Welsh, *Cancer Res.* **2009**, *69*, 1910 – 1915.
[22] S. Ahn, C. B. Duke III, C. M. Barrett, D. J. Hwang, C.-M. Li, D. D. Miller, J. T. Dalton, *Mol. Cancer Ther.* **2010**, *9*, 2859 – 2868.
[23] G. La Regina, R. Bai, W. Rensen, A. Coluccia, F. Piscitelli, V. Gatti, A. Bolognesi, A. Lavecchia, I. Granata, A. Porta, B. Maresca, A. Soriani, M. L. Iannitto, M. Mariani, A. Santoni, A. Brancale, C. Ferlini, G. Dondio, M. Varasi, C. Mercurio, E. Hamel, P. Lavia, E. Novellino, R. Silvestri, *J. Med. Chem.* **2011**, *54*, 8394 – 8406.
[24] Z.-K. Wan, S. Wacharasindhu, C. G. Levins, M. Lin, K. Tabei, T. S. Mansour, *J. Org. Chem.* **2007**, *72*, 10194 – 10210.
[25] M. Mateu, A. S. Capilla, Y. Harrak, M. D. Pujol, *Tetrahedron* **2002**, *58*, 5241 – 5250.
[26] W. J. Houlihan, G. Cooke, M. Denzer, J. Nicoletti, *J. Heterocycl. Chem.* **1982**, *19*, 1453 – 1456.
[27] S. Ghosh, M. Lobera, D. Schmidt, E. Baloglu (Tempero Pharmaceuticals, Cambridge, MA, USA), Int. PCT Pub. No. WO 2013/006408A1, **2013**.
[28] T. Mosmann, *J. Immunol. Methods* **1983**, *65*, 55 – 63.
[29] T. Müller, W. Voigt, H. Simon, A. Frühauf, A. Bulankin, A. Grothey, H.-J. Schmoll, *Cancer Res.* **2003**, *63*, 513 – 521.
[30] K. T. Papazisis, G. D. Geromichalos, K. A. Dimitriadis, A. H. Kortsaris, *J. Immunol. Methods* **1997**, *208*, 151 – 158.
[31] H. Y. Yamada, G. J. Gorbsky, *Mol. Cancer Ther.* **2006**, *5*, 2963 – 2963.
[32] C. Kanthou, G. M. Tozer, *Blood* **2002**, *99*, 2060 – 2069.
[33] R. B. Ravelli, B. Gigant, P. A. Curmi, I. Jourdain, S. Lachkar, A. Sobel, M. Knossow, *Nature* **2004**, *428*, 198 – 202.
[34] O. Trott, A. J. Olson, *J. Comput. Chem.* **2010**, *31*, 455 – 461.
[35] F. Bellina, S. Cauteruccio, S. Monti, R. Rossi, *Bioorg. Med. Chem. Lett.* **2006**, *16*, 5757 – 5762.
[36] M. Botta, S. Forli, M. Magnani, F. Manetti, in *Topics in Current Chemistry, Vol. 286* (Eds.: T. Carlomagno, K.-H. Altmann), Springer-Verlag, Berlin Heidelberg, **2009**, pp. 279 – 328.
[37] J. P. Gallivan, D. A. Dougherty, *Proc. Natl. Acad. Sci. USA* **1999**, *96*, 9459 – 9464.
[38] D. A. Dougherty, *J. Nutr.* **2007**, *137*, 1504S – 1508S.
[39] E. Aranda, G. I. Owen, *Biol. Res.* **2009**, *42*, 377 – 389.
[40] J. Bauer, M. Margolis, C. Schreiner, C. J. Edgell, J. Azizkhan, R. L. Juliano, *J. Cell. Physiol.* **1992**, *153*, 437 – 449.
[41] B. Nitzsche, C. Gloesenkamp, M. Schrader, M. Ocker, R. Preissner, M. Lein, A. Zakrzewicz, B. Hoffmann, M. Höpfner, *Br. J. Cancer* **2010**, *103*, 18 – 28.
[42] S. J. Lunt, S. Akerman, S. A. Hill, M. Fisher, V. J. Wright, C. C. Reyes-Aldasoro, G. M. Tozer, C. Kanthou, *Int. J. Cancer* **2011**, *129*, 1979 – 1989.
[43] PRODRG: A tool for high-throughput crystallography of protein – ligand complexes. A. W. Schüttelkopf, D. M. F. van Aalten, *Acta Crystallogr. Sect. D* **2004**, *60*, 1355 – 1363.
[44] J. Gasteiger, M. Marsili, *Tetrahedron* **1980**, *36*, 3219 – 3228.
[45] W. DeLano, The PyMOL Molecular Graphics System, DeLano Scientific LLC, San Carlos, CA (USA), **2003**.

Received: December 16, 2013
Published online on ■■ ■■, 0000

Variations on a promising theme: Tumor blood vessels are a good therapeutic target because they are fundamentally different from normal vasculature. This study shows that vascular-disrupting agents derived from verubulin have enhanced selectivity for cancer cells and lower general in vivo toxicity, yet they retain the strong antivascular activity of the lead compound.

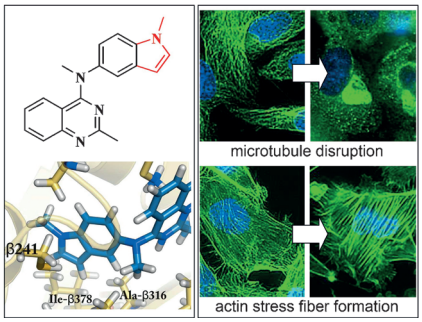

K. Mahal, M. Resch, R. Ficner, R. Schobert, B. Biersack, T. Mueller**

■■ – ■■

Effects of the Tumor-Vasculature-Disrupting Agent Verubulin and Two Heteroaryl Analogues on Cancer Cells, Endothelial Cells, and Blood Vessels